Optical breakdown processing: Influence of the ambient gas on the properties of the nanostructured Si-based layers formed

D.-Q. Yang, A. V. Kabashin, V.-G. Pilon-Marien, E. Sacher,[a] and M. Meunier
Groupe des Couches Minces and Département de Génie Physique, Ecole Polytechnique, C.P. 6079, succursale Centre-Ville, Montréal, Québec H3C 3A7 Canada

(Received 27 October 2003; accepted 17 February 2004)

Porous nanostructured layers, exhibiting 2–2.2 eV photoluminescent (PL) emission, have been formed on silicon surfaces by the production of optical breakdown in different gases (air, Ar_2, He,N_2, O_2), maintained at atmospheric pressure. We found a significant influence of the ambient gas characteristics on the morphological and chemical properties of the layers produced, as well as on the PL efficiency. Gases with relatively low ionization potentials (air, N_2, O_2) were found to better support the optical discharge and to provide the strongest plasma-related heating of the substrate material. This led to considerable microstructural and composition modifications, which gave rise to the maximization of PL emissions. In particular, for O_2, with the lowest ionization potential, we observed local plasma-provoked melting of the target surface and the disappearance of the porous structure of the layer. We also found a clear correlation between the PL properties of the layers, subsequent to fabrication, as well as after prolonged aging, and the presence of different oxygen-containing compounds. The structures produced are of importance for optoelectronics and biosensing applications. © *2004 American Institute of Physics.* [DOI: 10.1063/1.1702102]

I. INTRODUCTION

Due to the ability of Si nanostructures to emit visible light, such Si-based materials have been extensively studied for over two decades (Ref. 1 and references therein). Various methods have been proposed for the fabrication of these materials, including the direct processing of silicon wafers by wet anodic etching[1] and the deposition of thin, nanostructured Si-based films by various techniques.[2–13] Potential applications of such materials include biosensing[14] and Si-based photonics,[15] which take advantage ''dry'' methods for silicon nanostructure formation. Canham[1] proposed that the photoluminescent (PL) emission of Si, during dissolution, is associated with quantum size effects, in which the dissolution ultimately leads to the dimensions of the Si, lying between the pores, being reduced to quantum dots, permitting the two-dimensional quantum confinement of carriers. Although quantum confinement is in agreement with much of the experimental PL data,[1,2,4–13] this is certainly not the primary mechanism in those cases where the defect states responsible for the PL are deep inside the oxide shell, or lie at the SiO_x/Si interface,[3,16–20] or involve surface electronic states,[21] or possess surface hydride or hydroxide complexes.[22]

However, only a few dry processing methods are known that make possible local nanostructure formation at the semiconductor surface, a process that is important for the creation of some industrially important materials. One such method is electrical spark processing, which permits the formation of local, porous, nanostructured layers on silicon wafers.[23–25] In addition, we recently used various laser-assisted processes to treat semiconductors,[26–28] in ambient air, to produce such nanostructures. The most efficient modification of semiconductor structural and photoluminescent properties was obtained with the use of IR radiation (10.6 μm) from a CO_2 laser. In this case, the optical breakdown of air took place, in which a plasma discharge was formed, absorbed the radiation power and propagated it into the cold ambient gas.[29] Being heated to temperatures over 10^4 K, this plasma modified the Si surface and led to the formation of porous layers exhibiting strong, uniform PL signals around 2 eV.[27,28] In contrast, in the case of UV radiation, the gas breakdown was absent, and the simple radiation-related ablation and redeposition of material took place, which led to spike-like surface morphologies and much weaker and nonuniform PL.[28]

Nevertheless, many aspects of breakdown processing remain unclear. In particular, the role of plasma-related processes in the formation of surface modifications has not yet been clarified. In addition, the microstructural and chemical properties of layers, during and after treatment, have not yet been studied.

Here, we consider optical breakdown, taking place in ambient gases with substantially different characteristics, to study the morphological, chemical and PL properties of layers which are formed on silicon as the result of the breakdown-related treatment. In addition, we consider modifications of properties of the layers after their prolonged aging in ambient air.

II. EXPERIMENT

The surface treatments were carried out using a Lumonics pulsed transverse excited atmospheric CO_2 laser (10.6 μm), having a pulse energy of ~1 J, a pulse duration of 1 μs full width at half maximum (FWHM), and a repetition rate of

[a]Author to whom correspondence should be addressed; electronic mail: edward.sacher@polymtl.ca

TABLE I. Summary of Si surface microstructures, chemical states and PL changes on the CO_2 laser optical breakdown of different gas environments.

	1st Ionization energy (eV)[a]	Microstructure		Oxidation			PL	
		Pores	Morphology	Si $2p$[c]	O $1s$[c]	FWHM[e]/ν (Si–O–Si)	Peak position (eV)	Integral intensity (a.u.)[d]
O_2	13.6	Not visible	Glassy, ripples	104.5	533.8	236	1.95–2	1.0
Air	14.3[b]	Visible	Porous, ripples	103.7	533.0	174	2–2.1	0.93
N_2	14.5	Visible	Porous, rough hillocks	103.5	532.7	100	2.1–2.15	0.95
Ar	15.8	Visible	Porous, ripples containing hillocks	103.1	532.5	85	2–2.1	0.84
He	24.6	Visible	Porous, ripples containing hillocks	⋯	⋯	⋯	2–2.1	0.4
Vacuum	⋯	Not visible	Glassy, cones, cracks	⋯	⋯	⋯	⋯	⋯

[a]Reference 44.
[b]Average ionization estimated from the values for N_2 (80%) and O_2 (20%).
[c]XPS peak position calibration: C $1s$ (C–C)=285.0 eV.
[d]Normalized to sample processed in O.
[e]Full width at half maximum of the Si–O–Si stretching peak at ~1070 cm^{-1}.

3 Hz. The laser was focused by a Fresnel lens, whose focal length was about 15 cm. The pulsed laser surface modifications of Si were performed in a turbopumped vacuum chamber, at room temperature, at a base pressure lower than 5×10^{-5} Torr. The chamber could easily be backfilled with any of several super-high purity gases, such as O_2, N_2 or Ar. The air environment to which the sample was also exposed was at a relative humidity of 30%.

The Si wafers used, both *n* and *p* type, with resistances of 0.01–10 Ω cm, were fragmented into pieces 1 cm on a side, before being subjected to laser irradiation. Samples were held vertically, perpendicular to the laser beam; both *n*- and *p*-type samples gave similar results.

The PL measurements, microstructural analyses and surface compositions were determined after 900 laser pulses. The PL spectra were measured at room temperature, using an Instruments SA model U100 double beam spectrometer and a Hamamatsu Photonics GaAs photomultiplier. The samples were illuminated by a 488 nm INNOVA model 100 continuous wave, Ar^+ laser. A scanning electron microscope (SEM, Philips model XL20) was used to examine the target surface.

X-ray photoelectron spectroscopic (XPS) analysis took place in a VG ESCALAB 3 Mark II, using a nonmonochromated Mg K_α x-ray source, at 1253.6 eV, at a base pressure below 10^{-10} Torr. Spectral peaks were separated using the VG Avantage program, and Shirley background removal was employed. High-resolution spectra were obtained at a perpendicular takeoff angle, using a pass energy of 20 and 0.05 eV steps. All peaks were calibrated by setting the C $1s$ hydrocarbon contaminant peak to 285.0 eV.

Photoacoustic Fourier transform infrared (FTIR) spectroscopic data were obtained using a He-purged MTEC 300 photoacoustic cell in a Bio-Rad FTS 3000 spectrometer. The 2.5 kHz modulation frequency used probed the entire sample thickness.

III. RESULTS

A. Fabrication

We found that the threshold number of pulses for gas breakdown initiation was different for each gas, as discussed in Sec. C, below. The lowest threshold was observed for O_2, followed by air, N_2, and Ar. For He, with the highest ionization potential, the plasma discharge in ambient gas was very weak, and the plasma formed was localized near the focal spot on the target surface. In contrast, the other gases were characterized by the presence of obvious plasma discharges. These discharges manifested themselves as linear bright flashes, moving from the target surface toward the focusing lens. Under constant laser fluence, the visible intensity of the discharge, and the distance of its propagation, depended on the gas ionization potential; values are found in Table I. The maximum intensity and the largest plasma volume were observed for O_2, and the distance of discharge propagation for this gas could reach 1.5–2 cm from the target. The intensity of this discharge rose progressively with the number of laser pulses, stabilizing only after, e.g., 10–20 pulses in air. The intensity increase was related to the appearance of morphological defects on the target surface, whose appearance in-

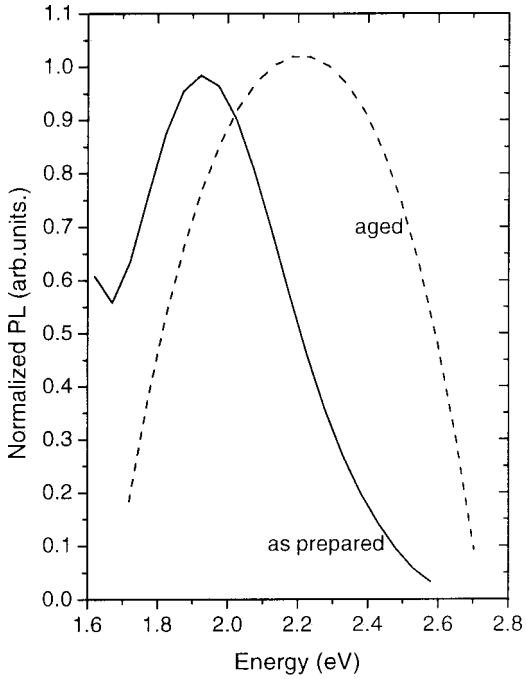

FIG. 1. Photoluminescence spectral changes of Si, on treatment by O_2, and after aging in air for one month.

creased the radiation absorption. Our experiments were carried out near the threshold of plasma production so as to minimize the size of the treated area.

B. PL behaviors in gas environments

On breakdown initiation, a gray-tinted area was formed at the focal point on the Si surface. Once exposed to air, this area exhibited strong PL signals, which could easily be seen by the naked eye; as found in many other studies (see, e.g., Refs. 20, 21), such materials do not manifest PL until exposed to air. Such exposure, over so short a time, serves only to oxidize the outer surface area.

The PL peaks are similar to those found in the literature; except for the case of O_2, Fig. 1, they are not shown. The strongest PL intensity was observed for those layers prepared in O_2, followed by those prepared in air, N_2 and Ar. For all the gases, the PL peak energy, just after layer fabrication, was ~2 eV (Table I), although, the energy for O_2 was slightly redshifted (1.95–2.0 eV), while that for N_2 was slightly blueshifted (2.1–2.15 eV). No significance is attached to these slight differences in peak maxima, since those of similar samples have been shown to depend on nanocluster size,[30,31] to which the present variations are attributed. However, stronger PL was found for samples treated in O_2, N_2 and air, indicating that the PL intensity is related to the plasma discharge intensity. Relative peak intensities, normalized to that on O_2 treatment, are found in Table I.

We also measured the PL peak stability on air exposure after one month, during which time the oxidation penetrates deeply into the substrate subsurface. The aged PL spectra were independent of the gas environment used during the preparation, confirming the extent of subsurface oxidation. The peak positions were around 2.2 eV, similar to our previous finding[32] that air-treated Si suffers a slight blueshift over the same time period. The effect of aging on the PL peaks is shown in Fig. 1 for a sample treated in O_2.

Scanning electron microscopy (SEM) photomicrographs (not shown) indicate that the microstructures undergo no observable change.

C. Surface morphological changes

The surface microstructures induced by CO_2 laser treatment can be found in Fig. 2. For comparison purposes, we include the surface morphology of a sample similarly irradiated in vacuum when the gas breakdown phenomenon is absent; the time necessary for forming a sustained plasma plume for all the gases used was directly related to the ionization constant (Table I), rising from ~40 s for O_2 to ~200 s for Ar and He.

The main features found in the SEM images in Fig. 2 are the following:

For all gases but O_2, the layers formed were highly porous. For N_2 and air, the formation of the porous structure was accompanied by the appearance of additional microcones and weak ripples, as shown in Figs. 2(c) and 2(d). In contrast, for O_2, with the lowest ionization potential, porosity appeared to be absent, while the treated surface contained clearly visible traces of a molten material [Fig. 2(e)]. In this case, we observed uniform, well-aligned ripples, with separations of 10 μm, perpendicular to those produced in the early stages of laser treatment;[33] the initial structures produced in vacuum do not change direction. The formation of these ripples is in good agreement with laser-induced periodic surface structure predictions.[34,35]

Although there are differences in the structures introduced, which depend on the gas environments used, all are in the submicron range, and result in a large increase in the surface: volume ratio. On the other hand, the surface morphology produced in vacuum is noticeably different: square cracks, 100 μm on a side, appear on irradiation, with sharp microcones, over 5 μm in height, at their corners. Short descriptions are found in Table I.

We have found that the interaction of pulsed CO_2 laser radiation and the Si surface has two components: the optical absorption of the radiation at the Si surface, in the early stages, before a sustained plasma is achieved,[33] and the plasma etching and heating of the Si surface, after a sustained plasma is achieved; the latter plays an important role only on long-term irradiation. As previously noted, the formation time of sustained plasma is associated with the first ionization energy of the species.

D. Photoacoustic FTIR

Photoacoustic FTIR provides chemical information on the near surface (1–2 μm, depending on the material and the frequency). The main vibrational features observed are found in Fig. 3 for selected gases. Beside the broad O–H stretching vibration, associated with SiOH of the native oxide, peaking at ~3400 cm^{-1}, and the C–H_n contaminant stretching vibration of the native oxide, at 2800–3000 cm^{-1}, one finds the

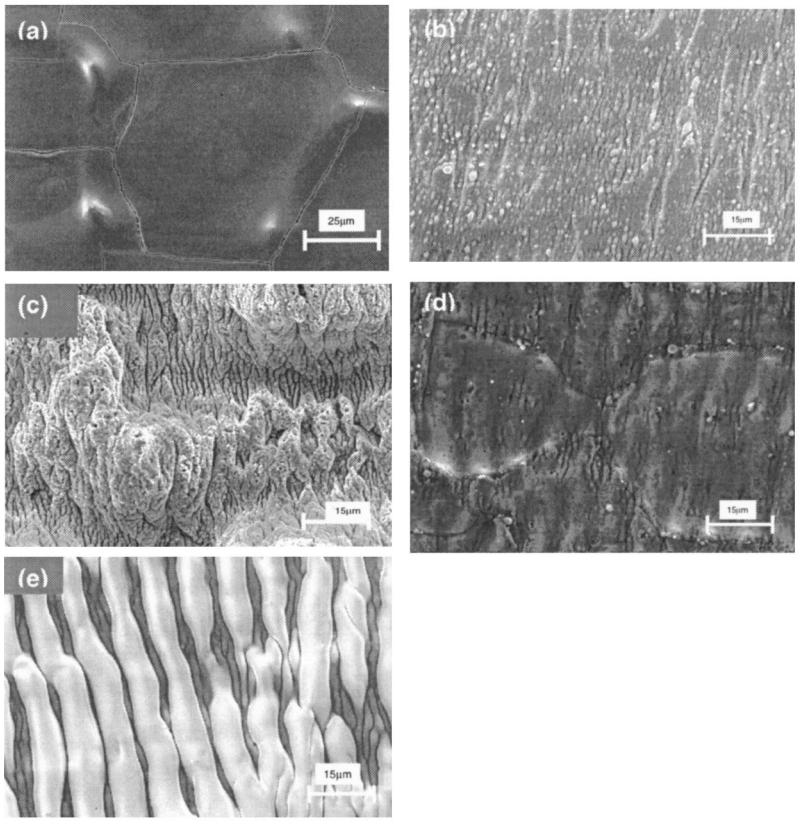

FIG. 2. SEM photomicrographs of Si processed in (a) vacuum, (b) Ar, (c) N_2, (d) air, and (e) O_2.

multicomponent Si–O–Si stretching peak at 1000–1250 cm^{-1}, seen in all cases, and the multicomponent Si–O–Si bending peak at 800–850 cm^{-1} peak. This latter peak is found, except for trace amounts, only after air and O_2 treatment, and appears to be associated with the higher energy component of the Si–O–Si stretching multiplet, whose peak is near 1100 cm^{-1}. The widths of the Si–O–Si peak for different gas environments are shown in Table I. One may see that the width increases as the ionization potential decreases, suggesting that the amount of oxygen in the treated layers is proportional to the plasma intensity during the treatment.

For the aged samples, significant spectral changes were found only in the case of O_2 treatment. The results on aging are found in Fig. 4 for O_2 treatment, with the spectrum normalized to the region above Si–O–Si stretching. Note that, in the case of O_2 treatment, substantial changes have occurred in the Si–O–Si region (1000–1250 cm^{-1}): the whole peak has decreased in amplitude *relative to changes in the O–H and C–H_n peaks* and, for the Si–O–Si stretching vibration, the shoulder at higher frequency (~1165 cm^{-1}) has decreased relative to the main component at ~1050 cm^{-1}. This latter change is attributed to a decrease in the Si:O ratio;[36,37] for example, Si oxidation states range from a Si

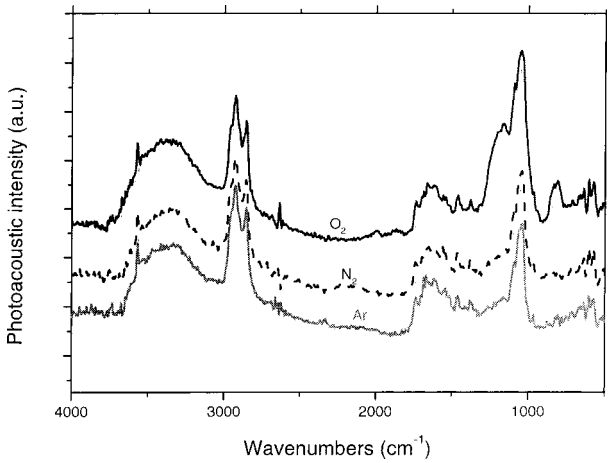

FIG. 3. Photoacoustic FTIR spectra of Si treated in several gas environments.

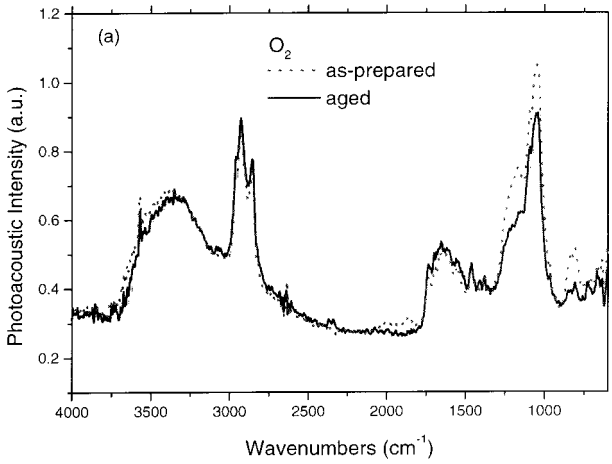

FIG. 4. Photoacoustic FTIR spectral changes of Si on treatment by O_2, after aging in air for one month.

atom surrounded by three Si atoms and one O atom (at the beginning of the oxidation process of pure Si), to a Si atom surrounded by four O atoms (c-SiO_2). The change in the Si–O–Si stretching region in Fig. 4 is due to the fact that air oxidation has caused less of an increase in the $\sim$1100 cm^{-1} component than in the $\sim$1000 cm^{-1} component; unfortunately, we are dealing here with amorphous SiO_x, where several components exist for which $x \leqslant 4$, and we do not know the specific reactions occurring on exposure to air. This change in the ratio of the Si–O–Si components is also reflected in the Si–O–Si bending peak at 800–850 cm^{-1}, where, as expected, the amplitude has decreased. The existence of several oxidation environments of the native oxide formed is also reflected in the measured FWHM of the Si–O–Si peak, found in Table I, which reflects the several oxygen-containing environments introduced by the gas. Our XPS results, in the next section, clarify the oxidation process.

The photoacoustic FTIR results permit one to relate the blueshift of the PL spectra to the additional aging-related oxidation of layers only for samples treated in oxygen; the resolution of our system was not sufficient to detect any significant spectral changes for samples prepared in the other gases during aging. Thus, at this point, it is difficult to make a definitive conclusion on the chemical origin of the blue PL shift.

E. XPS analysis

Further information on the extreme surface chemistry induced by the treatments can be obtained from XPS, which probes depths to, at most, several tens of nm, compared to photoacoustic FTIR, which probes to depths of $\sim$2 μm. XPS survey spectra for samples exposed to all the gas environments (not shown) indicate that N is easily incorporated on exposure to a N_2 gas environment and/or on air exposure.

High-resolution O 1s and Si 2p XPS spectra were obtained, and their peak positions are found in Table I. Their analysis confirmed the basic conclusions of the photoacoustic FTIR studies on the correlation of the oxygen content in the layers formed on treatment, and the plasma intensity during the treatment. While we make no attempt to separate peaks in these spectral envelopes because of our uncertainty of the chemical structures involved, it is clear that the Si 2p doublet increases in magnitude and shifts from a maximum at $\sim$103 eV (majority $Si–Si(O_3)$ structure) to $\sim$104.5 eV (majority $Si(O_4)$ structure) as the O_2 content of the environment increases; similarly, the O 1s peak increases in magnitude, becomes obviously multicomponent and shifts from $\sim$532.5 to $\sim$534 eV. This is in agreement with the photoacoustic FTIR results (see Sec. D, above), where the increase in absorption in the Si–O–Si region (1000–1250 cm^{-1}) of Fig. 4 is directly related to the amount of O_2 in the treatment gas; here, it is clear that the increase on treatment in O_2, over that on treatment in air, is due to the increased production of the $Si(O_4)$ structure over the $Si–Si(O_3)$ structure. Further, it identifies the source of the Si–O–Si stretching peak at $\sim$1100 cm^{-1} as coming from a higher oxidation state environment. There is no evidence of the existence of Si^0 within XPS information depth of $\sim$10 nm in SiO_2.

The C 1s contaminant peak of the N_2-treated Si, not shown, manifests multiple C–N and C–O components above 285 eV, as well as a C–Si component at $\sim$283 eV; the oxidized carbon content of the contaminant layer and its reaction with the Si substrate were previously discussed by us, in our consideration of Si wafer contamination.[38] The N 1s peak of the same N_2-treated sample, not shown, manifests a highly oxidized component at $\sim$403 eV. These results imply that some C has bonded to both N and O, explaining the multiplicity of peaks in the 1500–1800 cm^{-1} region in Fig. 3

IV. DISCUSSION

The results presented in the previous sections of this article have been collected in Table I. The reader may wish to consult the table during the development of the present section.

The interaction of the IR laser pulse with matter has received much attention (for a review, see Ref. 29). In contrast to UV radiation, IR radiation is well absorbed by the plasma itself through the inverse bremsstrahlung mechanism. In a gas, at atmospheric pressure, the target first provides electrons to initiate the gas breakdown, which extends toward the focusing lens, absorbing the main IR radiation power. As a result, the plasma becomes heated to temperatures of about 10^4 K, and can modify material properties.

We reason that the breakdown treatment process consists of two stages.[27] The first one takes place at the first moments of radiation-matter interaction, before the formation of a highly absorbent plasma discharge that prevents the transfer of radiation power to the target surface. During this stage, the radiation power is absorbed at the silicon wafer surface, which leads to the radiation-related melting and flash evaporation of the target material.

It should be noted that CO_2 laser radiation is only weakly absorbed by silicon, itself. While local surface defects, arising on the target surface as a result of the gas optical breakdown processing, are also known to significantly improve radiation absorption,[27] we recently showed[33] that the absorption improvement in the present case is due to chemical transformations at the sample surface (in the cases of air and oxygen, this material is mainly oxidized and, in any case, oxidation occurs on air exposure).

The second stage, occurring during and after the laser pulse, is characterized by the plasma-related heating of the material and, as a consequence, a modification of its properties occurs. The evolution of the surface morphology during laser treatment is probably governed by the interplay and competition among the dynamics of surface roughening, physical and chemical etching, melting and surface diffusion, which are induced by the electric field, the chemical potential, etc. We are, at present, not able to model these complex physical and chemical processes. However, it is clear that the properties of the layers produced were strongly dependent on the gas environment. Both morphology and chemical composition of the layers changed with a change of breakdown plasma intensity, which was ultimately determined by the ionization potential of the gaseous environment. At a given

pressure, the plasma intensity increases as the ionization energy decreases. The order of the decreasing interaction between the plasma and the Si surface should then be: O_2 $>$air$>N_2>$Ar, He, etc. In experiments with gases having relatively high ionization potentials, we observed the formation of a highly porous structure. We believe that the formation of this structure is due to the radiation-related evaporation and subsequent redeposition of material. Due to the nonuniform absorption of the radiation intensity, this process does not take place uniformly, which may cause the appearance of pores on the target surface. In contrast, for O_2 with the lowest ionization potential, the treated surface appeared molten, with the absence of pores (it may be that such pores do, in fact, exist but are too small to be seen with the instruments available to us). This melting, in the case of O_2, means that the temperature of the breakdown plasma becomes sufficiently high to melt the upper layers of the substrate. This result is very important since it unambiguously reveals the breakdown plasma-related contribution to the heating of the substrate and the modification of its properties. In the case of gases with intermediate ionization potentials (N_2,air), we observed the appearance of microcones and weak ripples in addition to the formation of the porous structure. The appearance of such structures is consistent with the nonuniform, incomplete melting of the porous substrate by the breakdown plasma. Thus, modifications of the surface substrate were principally due to different intensities of the breakdown plasmas for the different gases used.

The chemical composition of the layers produced also depends on the gas environment during the treatment. Our results showed that the use of gases with lower ionization potentials leads to a higher concentration of oxygen in the layers formed. We suggest that treatment by either laser or plasma provokes chemical changes at the substrate surface, along with the introduction of free radicals (also called dangling bonds) through the breaking of chemical bonds. The concentration of free radicals produced by the treatment will depend on the concentration of charged species in the plasma that attacks the surface and, as seen in Table I, O_2 has a significantly lower ionization potential than the other gases used here. While the photoacoustic FTIR technique gives no hint as to the extent of free radicals present, it is clear that they are formed by all the gas treatments. This is seen in Sec. III D, above, where the differences in aging show the effects of free radical reaction with the components of the atmosphere, such as O_2 and H_2O, and their reflection in the IR Si–O–Si stretching and bending regions in Fig. 3, as previously described (see Sec. III C, above). One must note that, despite the free radicals present at the surface before oxidation, PL is not manifested until exposure to atmosphere.

However, the mechanism of 2–2.2 eV PL is still not clear to us. It is evident that among those factors affecting the PL properties, we should exclude the surface microstructure since quite different morphologies, as shown in Fig. 2, lead to the generation of the same PL band. In addition, the microstructure (see Sec. III C, above) does not change with aging, while the PL peak position (see Sec. III B, above) does. However, the structure of the layers in the nanoscale level could still be a factor, which influences or even determines PL properties. As we have recently shown, the layers produced consist mainly of Si nanocrystals embedded in the oxide matrix.[27] The presence of nanocrystals may contribute to PL through the carrier confinement mechanism.[1] While the obviously melted and quenched surface of Si treated by O_2 [Fig. 3(c)] makes the existence of nanocrystals questionable, a recent article,[39] using conventional pulsed laser ablation, demonstrated the existence of Si nanocrystals too small to be seen by the high-resolution transmission electron microscope those researchers used. The presence of a blueshift of the PL spectra of all samples, on aging (see Sec. III B, above), is also consistent with the quantum confinement mechanism. Indeed, the previously mentioned increase of the oxygen content during aging may be accompanied by a decrease of the Si nanocrystal size in the SiO_x matrix, which might lead to the blueshift of the PL peak according to the quantum confinement model, as was observed in several studies (see, e.g., Refs. 2, 4, 5, 10).

Nonetheless, other mechanisms could be also responsible for the observed PL signals. In the case of O_2, the absence of Si^0 suggests that the PL may not be related to quantum confinement. Further, it is known[40] that the large stress induced on the oxidation of c-Si to a-SiO_x is sufficient to break chemical bonds in the oxide and, thus, form defects in the SiO_2 matrix, which can also exhibit PL in 2.0–2.4 range,[41] and is attributed to a nonbridging oxygen hole, consistent with our XPS and FTIR data; in this case, the blue PL shift on aging in air may be related to the larger stress introduced by the prolonged oxidation. The blueshift on aging, after N_2 plasma exposure, confirms previous findings.[42,43]

One may ask if there is any one overarching PL mechanism fitting *all* the gas environments used here. If so, the material involved in the mechanism must be present in all cases, although slightly varying from cases to case (as are the PL peaks and intensities in Table I). One such material is the native oxide *subsequent to air exposure*. (Prior to gas treatment, the native oxide does not have a PL spectrum.) However, as seen in the photoacoustic FTIR spectra in Fig. 3, the chemical changes on treatment do not suggest a chemistry that might give rise to PL. Thus, while we cannot presently point to a definite cause for PL in gas-treated Si, our results clearly show that the higher plasma temperature in the O_2 gas environment results in extensive melting and greater oxidation than in air, N_2, etc., environments; these latter environments evidence porosity and incomplete melting by their plasmas. Therefore, we are led to the limited conclusion that the efficiency is related to the extent of oxidation of the nanolayers produced.

V. CONCLUSIONS

Si wafer processing by CO_2 laser, in several gas environments, has resulted in microstructural and chemical changes at the surface. These changes have been used to show that surface chemistry and the presence of free radical-related oxygen hole centers both contribute to PL properties. Further, while the components of air do not appear to be implicated in the source of PL, they influence the PL peak positions and shapes.

ACKNOWLEDGMENTS

The authors thank the Natural Sciences and Engineering Research Council of Canada for funding, Professor Richard Leonelli, Université de Montréal, for his assistance with PL measurements, and J. E. Klemberg-Sapieha, École Polytechnique de Montréal, for discussions.

[1] L. T. Canham, Appl. Phys. Lett. **57**, 1046 (1990).
[2] H. Takagi, H. Ogawa, Y. Yamazaki, A. Ishizaki, and T. Nakagiri, Appl. Phys. Lett. **56**, 2379 (1990).
[3] Y. Kanemitsu, T. Ogawa, K. Shiraishi, and K. Takeda, Phys. Rev. B **48**, 4883 (1993).
[4] E. Edelberg, S. Bergh, R. Naone, M. Hall, and B. S. Aydil, Appl. Phys. Lett. **68**, 1415 (1996).
[5] M. Ehbrecht, B. Kohn, F. Huisken, M. A. Laguna, and V. Paillard, Phys. Rev. B **56**, 6958 (1997).
[6] E. Werwa, A. A. Seraphin, L. A. Chiu, C. Zhou, and K. D. Kolenbrander, Appl. Phys. Lett. **64**, 1821 (1994).
[7] I. A. Movtchan, R. W. Dreyfus, W. Marine, M. Sentis, M. Autric, G. Le Lay, and N. Merk, Thin Solid Films **255**, 286 (1995).
[8] Y. Yamada, T. Orii, I. Umezu, S. Takeyama, and T. Yoshida, Jpn. J. Appl. Phys., Part 1 **35**, 1361 (1996).
[9] T. Makimura, Y. Kunii, and K. Murakami, Jpn. J. Appl. Phys., Part 1 **35**, 4780 (1996).
[10] L. Patrone, D. Nelson, V. I. Safarov, M. Sentis, W. Marine, and S. Giorgio, J. Appl. Phys. **87**, 3829 (2000).
[11] A. V. Kabashin, M. Meunier, and R. Leonelli, J. Vac. Sci. Technol. B **19**, 2217 (2001).
[12] A. V. Kabashin, J.-P. Sylvestre, S. Patskovsky, and M. Meunier, J. Appl. Phys. **91**, 3248 (2002).
[13] T. Yoshida, S. Takeyama, Y. Yamada, and K. Mutoh, Appl. Phys. Lett. **68**, 1772 (1996).
[14] L. Pavesi, L. Dal Negro, C. Mazzoleni, G. Franzo, and F. Priolo, Nature (London) **408**, 440 (2000).
[15] V. S.-Y. Lin, K. Motesharei, K. P. S. Dancil, M. J. Sailor, and M. R. Ghadiri, Science **278**, 840 (1997).
[16] S. M. Prokes and W. E. Carlos, J. Appl. Phys. **78**, 2671 (1992).
[17] L. N. Dinh, L. L. Chase, M. Balooch, L. J. Terminello, and F. Wooten, Appl. Phys. Lett. **65**, 3111 (1994).
[18] T. Torchynska, J. Aguilar-Hernandez, A. I. D. Cano, G. Contreras-Puente, F. G. B. Espinoza, Y. V. Vorobiev, Y. Goldstein, A. Many, J. Jedrzejewski, B. M. Bulakh, and L. V. Scherbina, Physica B **308**, 1108 (2002).
[19] Y. Kanemitsu, T. Matsumoto, T. Futagi, and H. Mimura, Mater. Res. Soc. Symp. Proc. **298**, 205 (1993).
[20] K. S. Min, K. V. Shcheglov, C. M. Yang, H. A. Atwater, M. L. Brongersma, and A. Polman, Appl. Phys. Lett. **69**, 2033 (1996).
[21] M. V. Wolkin, J. Jorne, P. M. Fauchet, G. Allan, and C. Delerue, Phys. Rev. Lett. **82**, 197 (1999).
[22] M. S. Brandt, H. D. Fuchs, M. Stutzmann, J. Weber, and M. Cardona, Solid State Commun. **81**, 307 (1992).
[23] R. E. Hummel and S.-S. Chang, Appl. Phys. Lett. **61**, 1965 (1992).
[24] E. F. Steigmeier, H. Auderset, B. Delley, and R. Morf, J. Lumin. **57**, 9 (1993).
[25] R. E. Hummel, A. Morrone, M. Ludwig, and S.-S. Chang, Appl. Phys. Lett. **63**, 2771 (1993).
[26] A. V. Kabashin and M. Meunier, Appl. Surf. Sci. **186**, 578 (2002).
[27] A. V. Kabashin and M. Meunier, Appl. Phys. Lett. **82**, 1619 (2003).
[28] A. V. Kabashin and M. Meunier, Mater. Sci. Eng., B **101**, 60 (2003).
[29] Yu. P. Raizer *Laser-Induced Discharge Phenomena* (Consultants Bureau, New York, 1977).
[30] L. K. Pan, C. Q. Sun, B. K. Tay, T. P. Chen, and S. Li, J. Phys. Chem. B **106**, 11725 (2002).
[31] C. Q. Sun, L. K. Pan, Y. Q. Fu, B. K. Tay, and S. Li, J. Phys. Chem. B **107**, 5113 (2003).
[32] A. V. Kabashin and M. Meunier, Appl. Surf. Sci. **168**, 328 (2001).
[33] D.-Q. Yang, E. Sacher, and M. Meunier, Appl. Surf. Sci. **222**, 365 (2004).
[34] M. Birnbaum, J. Appl. Phys. **36**, 3688 (1965).
[35] J. F. Young, J. E. Sipe, J. S. Preston, and H. M. van Driel, Phys. Rev. B **27**, 1141 (1983).
[36] E. Sacher, Philos. Mag. B **51**, 285 (1985).
[37] E. Sacher, Sol. Energy Mater. **13**, 441 (1986).
[38] M. K. Shi, E. Sacher, and M. Meunier, Proceedings of the Annual Meeting of the Adhesion Society, Adhesion Society, Inc., Blacksburg, VA, 1997, p. 385.
[39] T. Makino, Y. Yamada, N. Suzuki, and T. Yoshida, J. Appl. Phys. **90**, 5075 (2001).
[40] A. Ourmazd, D. W. Taylor, J. A. Rentschler, and J. Bevk, Phys. Rev. Lett. **59**, 213 (1987).
[41] S. Munekuni, T. Yamanaka, Y. Shimogaichi, K. Nagasawa, and Y. Hama, J. Appl. Phys. **68**, 1212 (1990).
[42] B. H. Augustine, E. A. Irene, Y. J. He, K. J. Price, L. E. McNeil, K. N. Christensen, and D. M. Maher, J. Appl. Phys. **78**, 4020 (1995).
[43] C. Wu, C. H. Crouch, L. Zhao, and E. Mazur, Appl. Phys. Lett. **81**, 1999 (2002).
[44] J. E. Huheey, *Inorganic Chemistry*, 2nd ed. (Harper & Row, New York, 1978), p. 40.